RSC Advances



This is an *Accepted Manuscript*, which has been through the Royal Society of Chemistry peer review process and has been accepted for publication.

Accepted Manuscripts are published online shortly after acceptance, before technical editing, formatting and proof reading. Using this free service, authors can make their results available to the community, in citable form, before we publish the edited article. This Accepted Manuscript will be replaced by the edited, formatted and paginated article as soon as this is available.

You can find more information about *Accepted Manuscripts* in the **Information for Authors**.

Please note that technical editing may introduce minor changes to the text and/or graphics, which may alter content. The journal's standard <u>Terms & Conditions</u> and the <u>Ethical guidelines</u> still apply. In no event shall the Royal Society of Chemistry be held responsible for any errors or omissions in this *Accepted Manuscript* or any consequences arising from the use of any information it contains.



Cite this: DOI: 10.1039/c0xx00000x

PAPER www.rsc.org/xxxxxx

Fe₃O₄ Nanopearls Decorated Carbon Nanotubes Stemmed from Carbon **Onions with Self-cleaning and Microwave Absorption Properties**

Xianyong Lu^{a*}, Yanzi Wu^{a‡}, Hongyan Cai^{a‡}, Xingyuan Qu^{a‡}, Lingmei Ni^a, Chao Teng^a, Ying Zhu^{a*}, Lei Jiang^{a,b}

5 Received (in XXX, XXX) Xth XXXXXXXXX 20XX, Accepted Xth XXXXXXXX 20XX DOI: 10.1039/b000000x

Electromagnetic wave absorbing materials with microwave absorption capacity in a wide frequency range and superhydrophobic surface are of great importance for their applications in stealth technology, particularly, in high humidity ambient. In this paper, Fe₃O₄ nanopearls decorated carbon nanotubes stemmed from onion carbons (CNOs/CNTs@Fe₃O₄) have been successfully fabricated by a 10 facile flame strategy at the brass foil as substrate and catalyst. The Fe₃O₄ nanopearls from the thermal decomposition of Iron (III) acetylacetonate were in-situ decorated on the carbon nanotubes stemmed from the ripening of self-assembly of carbon onions aggregates from incomplete combustion of ethanol. Notably, this nanocomposite film exhibited well-performed microwave absorption with wide absorption frequency in 6-18 GHz based on cooperation of the dielectric loss of carbon nanotube and magnetic loss of Fe₃O₄ nanoparticles. Furthermore, the nanocomposite film displays the superhydrophobic property and low adhesive force that make them good 15 candidates for water shedding stealthy materials.

1 Introduction

Page 1 of 6 RSC Advances

The Microwave absorbing materials that can absorb electromagnetic (EM) waves effectively and dissipate microwave 20 by interference, are in high demand at present because of the development of military stealth technology and the increased demand of electronic devices. Over the past decade, various EM materials have been developed for these purpose, they are generally classified into dielectric and magnetic loss, according to 25 their loss characteristics.² In general, typical dielectric loss materials include conducting polymers,^{3, 4} reduced graphene oxide, ⁵⁻⁸ carbon nanotube, ⁹⁻¹² ZnO, ^{13, 14} TiO₂, ¹⁵ BaTiO₃, ¹⁶ while magnetic loss materials have Fe₃O₄, ¹⁷ Co, ¹⁸ Ni, ¹⁹ and Fe₃Al²⁰ et al. Different from those, carbon onion and carbon nanotube 30 (CNTs) are reprehensive novel nanomaterials, possessing many fascinated properties like high specific surface area, thermal conductivity, mechanical properties and electron mobility. These properties make them as good candidates for EM microwave materials. Unfortunately, there are still some problems unsolved 35 as follows: (1) they have the poor magnetic loss performance, restricting the improvement of their absorbing properties. (2) Carbon nanotube as power form usually tend to aggregate and restack, leading to the obvious reduction of available surface area. Therefore, it is highly desirable to construct the there-40 dimensional CNTs as microwave absorbers due to their ultrahigh surface-to-volume ratio, which can provide. Furthermore, as for high-efficiency microwave absorbers, it is also required to combine dielectric with magnetic materials to achieve impedance match between the complex permittivity and permeability, thus 45 improving the absorbing property. It needs to construct novel hybrid nanostructures based on carbon nanomaterials and magnetic nanoparticles which can exhibit the excellent dielectric polarization, magnetic loss performance and interface action

- 50 Fe₃O₄/Polyaniline, ²² Fe₃O₄/CNT²³, Fe₃O₄/Graphene²⁴. However, multi-step procedures involved in fabrication of these hybrid nanomaterials may limit its practical applications. Therefore, it is urgent to develop a facile and large-scale strategy for fabricating nanocomposites for high-efficiency microwave absorption.
- In practical applications, it is inevitable for microwave absorbers to encounter the high humidity environments that degrade conductivity of materials, thus leading to decrease microwave absorbing performance. There were some crashes of stealth fighters due to their poor water shedding capacity. Some 60 types of stealth fighters even had to retire, because they lost the capacity of microwave absorbing in the rainy Superhydrophobic surfaces have extreme water repellency that remove quickly water from surface, thus may protect their conductivity. For example, Zhu et al reported a superhydrophobic 65 conductive, magnetic carbon nanofibers coating via a electrospinning method.²⁵ Megaridis et al presented a solventbased, mild method to fabricate superhydrophobic, carbon nanofiber/PTFE-filled polymer composite coatings for EMI shielding. ²⁶ Although some progress has been made in electromagnetic 70 fabrication of materials with superhydrophobicity, it is in great emergency to develop a facile strategy for preparing high performance microwave absorbing materials with excellent water-shedding property.

Herein, a facile one-step flame strategy has been well 75 developed to fabricate superhydrophobic CNOs/CNTs@Fe₃O₄ nanocomposite film on a large scale at the brass foil as substrate. The microwave absorbing nanocomposite film has well-defined three dimensional structures containing aligned carbon nanotubes decorated by magnetite nanopearls. The formations of CNTs 80 were from the ripening of carbon onions aggregates assemblies. This microwave absorbing nanocomposite exhibits high performance microwave absorbing capacity at a wide frequency

compared with the reported EM materials such as Fe₃O₄@TiO₂, ²¹

range. Moreover, the as-prepared nanocomposite film shows superhydrophobic property with contact angle (CA) of $155 \pm 1.6^{\circ}$ and a low-adhesion, which make them as promising candidate for water-shedding stealthy materials.

2 Experimental Sections

Materials

Iron (III) acetylacetonate (Fe(acac)₃) was purchased from Aldrich and used after a 2-fold recrystallization. Brass foil was obtained 10 from Goodtime Industry (Beijing) Limited. Copper foil (thickness 0.25 mm, 99.95+%) was from Sigma-Aldrich. Other chemical reagents with analytical grade were used as received.

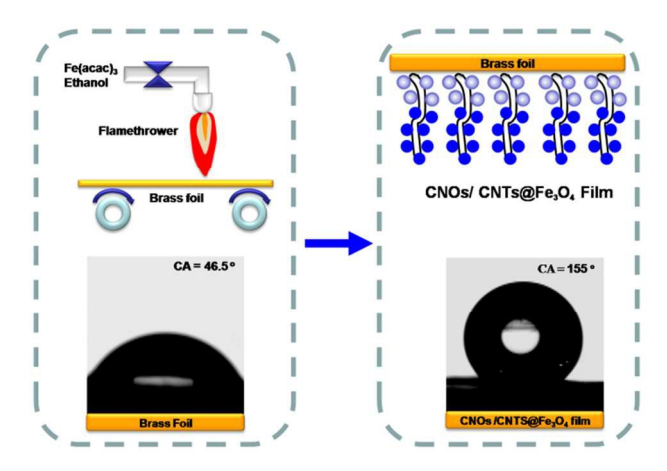
Preparation of aligned carbon nanotube decorated by Fe₃O₄ nanopearls

15 In a typical fabrication, Fe(acac)₃ was dissolved in ethanol with concentration of 0.4 mol/L. Then the Fe(acac)₃ solution was pumped to a fixed flamethrower at a certain speed from a raw material tank. After ignition of this solution, a brass foil was employed as substrate to collect nanocomposite s from the flame $_{20}$ of flamethrower. The reaction temperature was about 488.6 ± 3.5 °C. In order to obtain the large area film, brass foil could be fixed on a computer-controlled rolling device. The thickness of nanocomposite film could be controlled by deposition time and the moving speed of brass foil. The brass foil is hydrophilic with 25 CA of 46.5 \pm 1.2 $^{\circ}$. However, the brass foil with nanocomposited film exhibits superhydrophobicity with CA=155 \pm 1.6 °. The water droplets could easily slide off this surface. The fabricated process and wettability of CNTs@Fe₃O₄ aligned film is shown in

30 Characterizations

Scheme 1.

Scanning electron microscope (SEM) and Energy Dispersive Spectrometry (EDAX) studies were done with Hitachi S-4800 microscope and FEI Nova Nanolab SEM, respectively. Transmission electron microscope (TEM) images of the samples 35 were taken on a JEM-100CXII electron microscope at an acceleration voltage of 100 kV. High resolution TEM (HRTEM) was performed in JEOL 3011 High Resolution Electron Microscope with accelerating voltage of 300 KV. Powder X-ray diffraction (XRD) pattern of the particle samples was recorded on 40 a Regaku D/Max-2500 diffractometer under Cu Kα1 radiation (λ = 1.54056 Å). Roman spectra were recorded on a Jobin Yvon (Laboratory RAM HR800) confocal micro-Raman spectrometer backscattered geometry through a $10 \times (NA = 0.25)$ microscope objective. Ar+ laser emitting at a wavelength of 514.5 nm was 45 used as a source of excitation. CAs were measured on an OCA20 machine (DataPhysics, Germany) contact angle system at ambient temperature. The magnetic properties of the resultant samples were characterized by using a vibrating sample magnetometer (VSM JDM-13, China). High speed movies were 50 taken with a high speed camera (Phantom v9.1 vision research, America). X-ray photoelectron spectroscopy data were obtained with an ESCALab220i-XL electron spectrometer from VG Scientific using 300 W Mg KR radiation. The base pressure was about 3×10^{-9} mbar. A powder sample of composite material was 55 first mixed with an equal weight of olefin. Then, the resultant mixture was used to form an O-ring shaped sample (i.d. 3 mm, o.d. 7 mm, and thickness 2 mm) under the melting state of paraffin. The relative complex permittivity and the relative complex permeability were determined using a vector network 60 analyzer (Agilent N5230A) in the range of 2-18 GHz.



Scheme 1 Synthetic procedure of aligned Carbon Nanotubes decorated with Fe₃O₄ nanocomposite film via a flame strategy.

3 Results and discussions

Scheme 1 shows the synthetic procedure of nanocomposite film 65 via a simple flame strategy on a brass foil as a substrate. The method was based on the combustion of ethanol, in-situ thermal decomposition of Fe(acac)₃ and brass foil as substrate collecting the products on the out-flame of flamethrower. While the black film was formed on the brass foil, there was a sharp wetting ₇₀ transition from hydrophilic state with contract angle (CA) $46.5\pm$ 1.2 ° to a superhydrophobic state with CA of 155 \pm 1.6 °.

The morphology and detailed structures of the as-fabricated film and nanoparticles stripped from this film are investigated by SEM, TEM and HRTEM characterizations. From Fig 1 a, it can 75 be clearly observed that the film has three-dimensional (3D) structures. High resolution of SEM image indicated that that the film composed of the curved nanofibers decorated by many nanoparticles with average size of 48.0 ± 14.6 nm, as given in Fig. 1b and c. TEM image further indicated that the nanofibers are 80 hollow tubes that have the average length and diameter of 4.3 \pm 1.1 um and 19.4 ± 2.8 nm (Fig.1c). HRTEM image showed that the well-defined crystalline lattice spacing of 3.4Å attributable to (002) crystal plane of the carbon onions²⁷, while the crystal lattice of 3.8 Å is assigned to the nature of multi-walled carbon 85 nanotubes (Fig 1d and f), Furthermore, HRTEM image clearly demonstrates that the lattice fringe pitch of 4.9 Å corresponds well with the d-spacing of the (111) reflections for singlecrystalline nature of Fe₃O₄ (Fig. 1e). XRD pattern indicates that the broad diffraction peak located at 28 ° is corresponded to the 90 (002) plane of graphite which has inter-planar spacing of 3.4 Å (Fig. 1e).²⁸ Other six peaks indexed as the characteristic (220), (311), (400), (422), (511) and (440) are attributed to the Fe₃O₄ nanoparticles (JCPDF no. 88-0866), which agree well with the result of HRTEM.

95 Fig. 3 shows the Raman spectra of the nanocomposite film. It is observed that the G band centred at 1598 cm-1 indicates the nanocomposite film has the graphic sp² phase corresponding to the E_{2g} phonon mode at the Brillouin zone atom.² The in-plane bond stretching of sp²-bonded carbon atoms in as-prepared 100 nanocomposite film is also found, suggestive of some disordered graphic structures. The D band at 1350 cm⁻¹ indicates that breathing mode of the six-fold aromatic rings in carbon

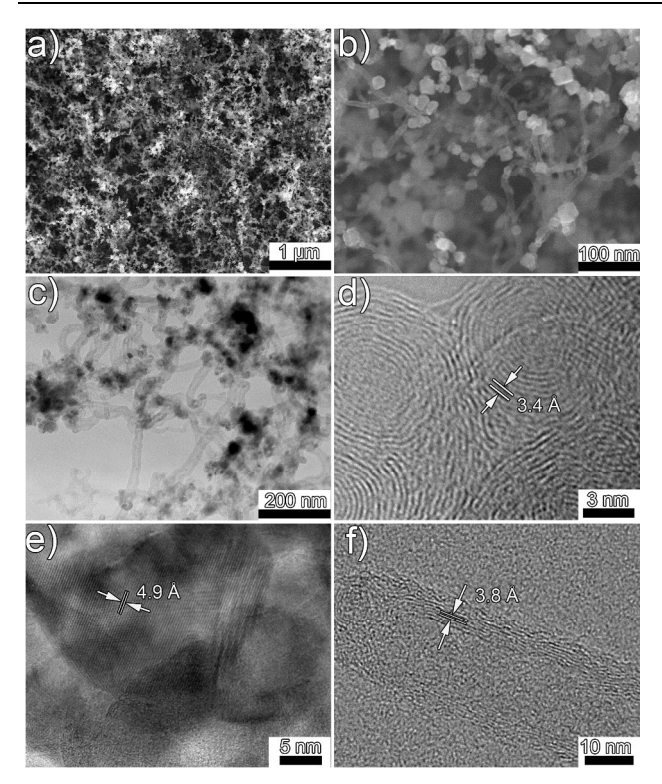


Fig 1. a) and b) SEM images of nanocomposite film with different magnifications, c) TEM image of sample striped from as-prepared film, d), e) and f) HR-TEM images of carbon onions, Fe₃O₄ nanoparticles, carbon nanotube in sequence.

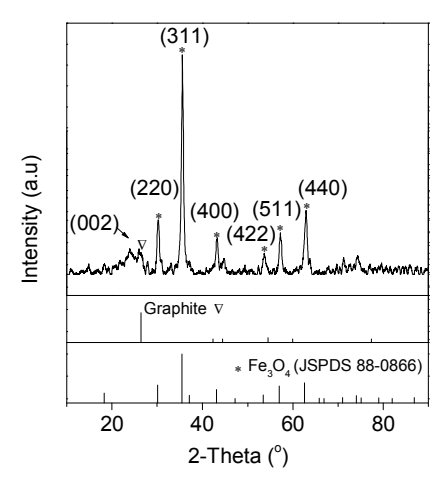


Fig 2. XRD patterns of CNTs@Fe₃O₄ nanocomposites obtained by a flame strategy.

 $_{5}$ network and is assigned to the photons of A_{1g} symmetry at the K point of the Brillouin zone. This mode indicates that as-prepared material presents the structural disorder like armchair edges of the carbon network. Generally, the growth in the D-band intensity is widely used to qualify the disorder. The ratio of D-band to G- $_{10}$ band intensity (I_D/I_G) is 0.69 which indicates that some disordered carbon exist in as-prepared nanocomposite materials. The dimensionless A band at about 1528 cm⁻¹ is interstitial carbon with sp³ linking outside or inside the planes of the aromatic rings,

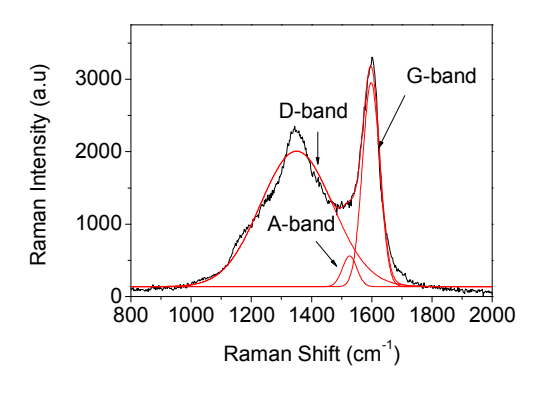


Fig 3. Raman spectrum of nanocompoistes striped from as-prepared superhydrophobic film.

which assigned to the amorphous carbon. ²⁹ The ratio of the intensity of A band to the intensity of G band (I_A/I_G) is 0.19 which supports that the carbon with amorphous structure presents in the obtained products.

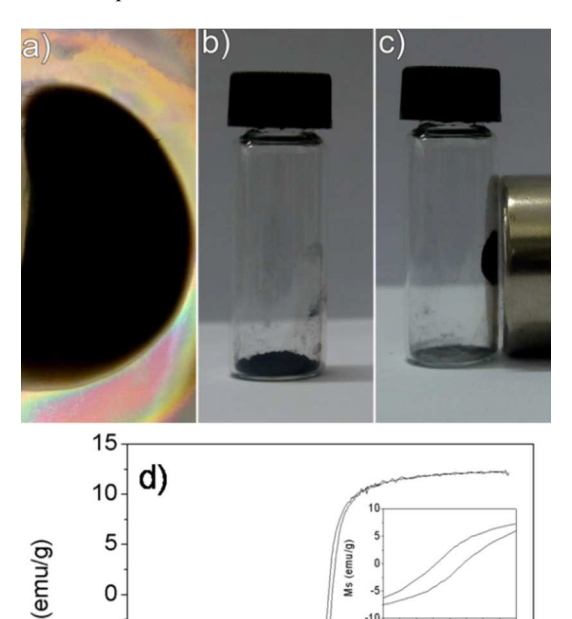


Fig 4. a) Photographs of nanocomposite film on brass foil, b) and c) nanocomposite sample stripped from this film captured in the absence or presence of a permanent magnet, Room-temperature magnetization curves nanocomposites by flame synthesis. Inset shows detailed view of room temperature magnetization of this sample.

Ó

H (Oe)

5000

10000

-5000

-5

-10

-10000

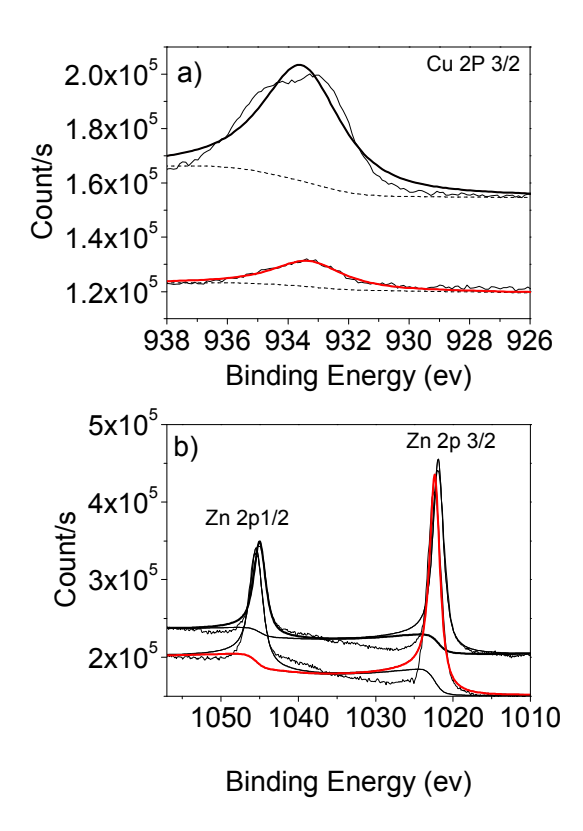


Fig 5. Survey X-ray photoelectron spectrum a) Cu 2p 3/2, b) Zn 2p 3/2 spectra of brass foil before (black lines) and after (Red lines) as substrate in the flame synthesis. The bold line show in frames are the best fits for Cu2p 3/2 and Zn 2p 3/2, respectively.

The magnetic property of the obtained composite film is also investigated (Fig 4). It can be seen that the composite materials 5 stripped from the brass substrate in the glass vessel can be easily attracted by a magnetic, suggesting the good magnetic properties of the composite film (Fig. 4a, 4b and 4c). Furthermore, vibrating sample magnetometer (VSM) data indicate that the composite film is paramagnetic with saturation magnetization (M_s) of 12.5 10 emu/g, coercivity (H_c) of 100.9 Oe and remnant magnetization(M_r) of 2.4 emu/g, respectively. The magnetic properties could be attributed to Fe₃O₄ nanoparticles in the composite film, which provide the magnetic loss for microwave absorbing materials.

It is generally accepted that the Fe₃O₄ nanoparticles in this film 15 were formed from thermal decomposition of Fe(acac)₃ via a flame strategy. However, the formation mechanism of CNOs and CNTs is still unclear. It is noticed that the composited film of CNOs/CNTs@Fe₃O₄ can form on the surface of the brass foil composed of Cu-Zn alloy with the molar ration of 2.1 to 1 (Fig. 20 S2). When the pure copper was used as substrate, only CNOs are found in the products (Fig. S1), no CNTs are observed in the products. It is easily concluded that the presence of element zinc in brass foil plays an important role in synthesis of CNTs@Fe₃O₄ nanocomposites film, especially for CNTs. To further understand 25 the formation mechanism, the fresh and used brass foils were detected by X-ray photoelectron spectroscopy (XPS). It is observed that the binding energies of Zn 2p_{3/2} and Cu 2p_{2/3} are 1021.9 eV and 933.5 eV, respectively, indicating the presence of the Zn⁰ and Cu²⁺ in the brass foil. However, after the brass foil

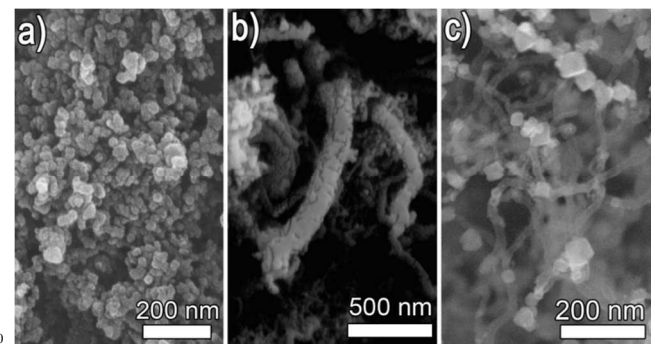
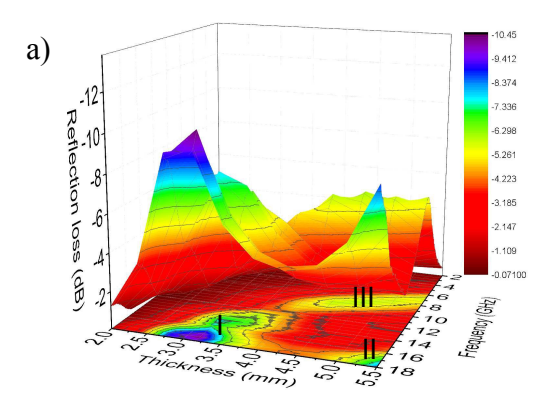


Fig. 6 SEM images of the products were collected at a) 30 min, b) 60 min, and c) 180 min, respectively.

was employed as substrate, the binding energy of Zn 2p_{3/2} is shifted to high value 1022.4 eV, suggestive of the formation of Zn^{2+} , but binding energy of Cu $2p_{2/3}$ has almost no change. This 35 result indicates that the presence of Zn⁰ in brass foil can contributed to the formation of CNTs in the composites film.

The multi-wall nature of CNTs is also investigated via varying the reaction time of 30 min, 60 min, and 180 min (Fig.6 a-c). It can be seen that at 30 min, the obtained products are spherical 40 CNOs aggregates with average size of 31.1± 6.2 nm. With prolonging reaction time, the CNOs aggregates had been assembly into nanofibers with relative loose structure at 60 min. When the reaction time prolong to 180 min, multi-wall CNTs were observed. Therefore, it is reasonable to deduce that the 45 CNTs were produced by ripening from the assemblies of nanotube-like structure of CNOs aggregates.

Due to the presence of CNOs, MCNTs and Fe₃O₄ nanoparticles, these nanocomposites can possess both magnetic and dielectric properties, thus making the film with special 50 electromagnetic absorption properties. The electromagnetic parameters (relative complex permittivity $\mathcal{E}_r = \mathcal{E} - j\mathcal{E}''$ and relative complex permeability, $\mu_r = \mu - j \mu$) of the wax composites containing 5 wt% of as-prepared nanocomposites were measured at room temperature. 24 The permittivity real part (55 ${\cal E}$), permittivity imaginary part (${\cal E}$), permeability real part (${\cal \mu}$), permeability imaginary part (μ), dielectric loss tangent ($\tan \delta \varepsilon$) and magnetic loss tangent ($\tan \delta \mu$) of the nanocomposites material are presented in Fig. 4s. For contrast, the CNOs/CNTs nanocomposites materials were obtained by 60 removing Fe₃O₄ nanoparticles from the as-prepared film materials via HCl (10 M). It is found that the \mathcal{E} values of CNOs/CNTs@Fe₃O₄ and CNOs/CNTs are decrease from 4.98 to 4.57 and from 5.74 to 4.72, respectively, with some fluctuations over 2-18 GHz frequency range (Fig. 4S a), while the E value 65 is changed from 0.62 to 0.44 and from 1.10 to 0.66, respectively, in the frequency range of 2-18 GHz (Fig. 4S b). The μ and μ values of CNOs/CNTs@Fe₃O₄ and CNOs/CNTs exhibit complex fluctuations in the frequency of 2-18 GHz (Fig. 4S c and 4S d). It is observed that when magnetic Fe₃O₄ nanoparticles are removed, 70 the μ and μ values decreased sharply due to low magnetic loss property. The dielectric tangent loss ($\tan \delta \varepsilon = \varepsilon''/\varepsilon'$) and the magnetic tangent loss ($\tan \delta \mu = \mu'' / \mu'$) were shown in Fig. 4S e and 4S f, respectively. It suggests that the sample A has strong dielectric loss against electromagnetic wave. By 75 removing of magnetic Fe₃O₄ nanoparticles, the CNOs/ CNTs nanocomposites have more ratio conducting materials than CNOs/CNTs@Fe₃O₄ nanocomposites materials. The strong



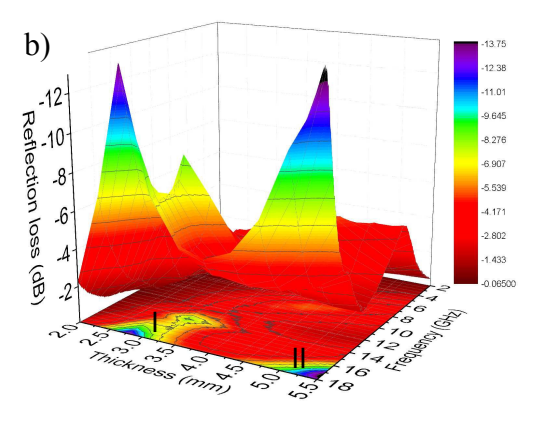


Fig 7. Microwave absorption properties of as-prepared nanocomposite film calculated by using the measured relative complex permittivity and permeability values according to transmission line theory. Three-dimensional microwave RL curves of the a) CNOs/CNTs@Fe₃O₄ n nanocomposites and b) CNOs/CNTs nanocomposites.

magnetic tangent loss ($\tan \delta \mu = \mu'' / \mu'$) of sample A indicated that CNOs/CNTs@Fe₃O₄ has more magnetic loss than s CNOs/ CNTs between 5 to 12.3, 15 to 18 GHz. These results 5 indicated that the electromagnetic absorption properties of CNOs/CNTs@Fe₃O₄ is originated from the coupling of the dielectric loss based on CNOs and CNTs and magnetic loss from Fe₃O₄ nanoparticles.

The reflection loss (R₁) values of the nanocomposites were 10 calculated according to the following equations. 30

$$R_L(dB) = 20\log\left|\frac{Z_{in} - 1}{Z_{in} + 1}\right|$$
 (1)

$$Z_{in} = \sqrt{\frac{\mu_r}{\varepsilon_r}} \tanh \left| j(2\pi f d/c) \sqrt{\varepsilon_r \mu_r} \right| \qquad (2)$$

Where Z_{in} is the input impedance of the absorber, f is the frequency of electromagnetic waves, d is the thickness of the 15 absorber, and c is the velocity of electromagnetic waves in free space. The impedance matching condition is determined by the combination of the six parameters: \mathcal{E} , \mathcal{E} , $\mathcal{\mu}$, $\mathcal{\mu}$, f and d. In order to study the influence of CNOs, CNTs and magnetite nanoparticles effect on the microwave absorbing, the calculated

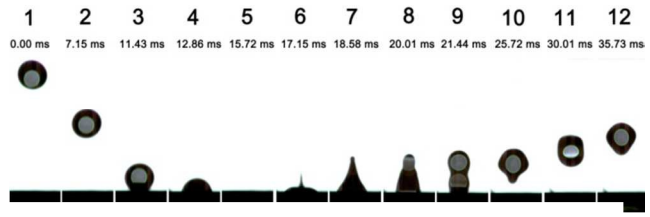


Fig. 8 Time-resolved images of the bouncing of a 5-μL water drop on superhydrophobic as-prepared microwave absorber film.

25 theoretical reflection loss of the CNOs/CNTs@Fe₃O₄ and CNOs/CNTs with filler loading of 5 wt% at different thickness in range of 2-18 GHz according to the equation 1 and 2.32 Fig. 7a and 8b show the RL of CNOs/CNTs@Fe3O4 and CNOs/CNTs. It can obviously observed that CNOs/CNTs@Fe3O4 has three 30 different microwave absorption areas including area I (thickness 2.5~4.5 mm, frequency 12~18 GHz), area II (thickness 4.5~5.5 mm, frequency 16~18 GHz) and area III (thickness 4.0 ~5.5 mm, frequency 6 ~12 GHz). By contrast, CNOs/CNTs has only two smaller absorption areas including area I (thickness 2.5~3.5 mm, 35 14~18 GHz) and area II (thickness 4.5 ~5.5 mm, frequency 16~18 GHz). According to the chemical difference between CNOs/CNTs@Fe₃O₄ and CNOs/CNTs, the magnetite nanoparticles in sample A is contributed to the wider frequency range for microwave absorption at lower thickness, but the film 40 has relatively good microwave absorption performance in the low frequency range. Notably, the as-prepared CNOs/CNTs@Fe₃O₄ nanoarray film exhibited the good microwave absorbing property both in low and high frequencies.

The superhydrophobic surface for microwave absorbing 45 nanocomposites film is also very important for their practical applications in civil and military. The as-prepared nanocomposites film exhibits the superhydrophobic property at wCA of 155 o in the air. It is necessary to study the interaction between the water droplet and this surface. Fig. 8 shows the time-50 resolved images of a water droplet bouncing on as-prepared CNOs, CNTs@Fe₃O₄ nanocomposites film well studied by a high speed camera. It was obviously observed that there was no any water residual during the bouncing process. The as-prepared nanocomposites film exhibited isotropic structures, which were $_{55}$ proved by the same value of sliding angle ($\sim 3^{\circ}$) under the different direction of this film. These results proved that this nanocomposites film with 3D structures exhibited the superhydrophobic property. Considering the microwave absorbing property and superhydrophobic wettability with low 60 adhesive property, this film may have future application in stealth materials with the capacity to absorb microwave signals with both high and low frequencies and excellent water shedding property.

Conclusions

65 In summary, a simple flame strategy is developed to construct the GNOs/CNTs@Fe₃O₄ nanoarray film on brass foil substrate. The brass foil that composes of Zn⁰ serves not only as the substrate, but also as the catalyst. CNOs were formed by incomplete combustion of ethanol, and then the tube-like 70 structures were obtained by the self-assembly of CNOs

aggregates. With the reaction proceeding, CNTs arrays were prepared by the ripening of the tube-like intermediates. At the same time, the Fe₃O₄ nanoparticles were produced from the thermal decomposition of Fe(acac)₃, which can in situ decorated 5 the CNTs. Furthermore, the as-prepared nanocomposites film exhibits the excellent microwave absorption capacity in a wider frequency and superhydrophobic wettability with low adhesive property. It is believed that the CNO/CNTs@Fe₃O₄ nanoarray film can be effective for applications in the water-shedding 10 stealthy materials.

Acknowledgments

The authors thank the financial support the Beijing Natural Science Foundation (2132030), the National Natural Science Foundation of China (21103006), China Scholarship Council 15 (201303070263), 863 Program (2012AA030305), Fundamental Research Funds for the Central Universities (YWF-10-01-B16, YWF-11-03-Q-214, YWF-13-DX-XYJL-004) and the 111 Project (No. B14009). The authors thank Prof. Dr. Nicholas. A Kotov of University of Michigan, Ann Arbor for his kind help 20 with HRTEM measurements.

Notes and references

- ^a Key Laboratory of Bio-Inspired Smart Interfacial Science and Technology of Ministry of Education, Beijing Key Laboratory of Bio-25 inspired Energy Materials and Devices, School of Chemistry and
- Environment, Beihang University, Beijing 100191, PR China E-mail: (X.Lu) xylu@buaa.edu.cn, (Y.Zhu) zhuying@buaa.edu.cn
- Institute of Chemistry, Chinese Academy of Sciences, Beijing 100190, P. R. China
- 30 [‡]These authors contributed equally to this work.
 - † Electronic Supplementary Information (ESI) available: [details of any supplementary information available should be included here]. See DOI: 10.1039/b000000x/
- 35 1 H. He and C. Gao, ACS Appl Mater Interfaces, 2010, 2, 3201-3210.
- 2. L. Wang, X. Jia, Y. Li, F. Yang, L. Zhang, L. Liu, X. Ren and H. Yang, J. Mater. Chem. A, 2014, 2, 14940-14946.
- 3. H. Ghasemi and U. Sundararaj, Synth. Met., 2012, 162, 1177-1183.
- 4. A. Ameli, M. Nofar, S. Wang and C. B. Park, ACS Appl. Mater. Interfaces, 2014, 6, 11091-11100.
- 5. M. Verma, A. P. Singh, P. Sambyal, B. P. Singh, S. K. Dhawan and V. Choudhary, Phys. Chem. Chem. Phys., 2015, 17, 1610-1618.
- 6. A. Joshi, A. Bajaj, R. Singh, P. S. Alegaonkar, K. Balasubramanian and S. Datar, Nanotechnology, 2013, 24, 455705-455708.
- 45 7. D.-X. Yan, P.-G. Ren, H. Pang, Q. Fu, M.-B. Yang and Z.-M. Li, J. Mater. Chem., 2012, 22, 18772-18774.
 - S. Kim, J.-S. Oh, M.-G. Kim, W. Jang, M. Wang, Y. Kim, H. W. Seo, Y. C. Kim, J.-H. Lee, Y. Lee and J.-D. Nam, ACS Appl. Mater. Interfaces, 2014, 6, 17647-17653.
- 50 9. S. Maiti, N. K. Shrivastava, S. Suin and B. B. Khatua, ACS Appl. Mater. Interfaces, 2013, 5, 4712-4724.
 - M. H. Al-Saleh and U. Sundararaj, Carbon, 2009, 47, 1738-1746. 10.
 - A. P. Singh, B. K. Gupta, M. Mishra, Govind, A. Chandra, R. B. Mathur and S. K. Dhawan, *Carbon*, 2013, 56, 86-96.
- 55 12. J.-M. Thomassin, X. Lou, C. Pagnoulle, A. Saib, L. Bednarz, I. Huynen, R. Jerome and C. Detrembleur, J. Phys. Chem. C, 2007, 111, 11186-11192.
 - 13. R. F. Zhuo, H. T. Feng, J. T. Chen, D. Yan, J. J. Feng, H. J. Li, B. S. Geng, S. Cheng, X. Y. Xu and P. X. Yan, J. Phys. Chem. C, 2008, 112, 11767-11775.
- 14. H. Li, Y. Huang, G. Sun, X. Yan, Y. Yang, J. Wang and Y. Zhang, J. Phys. Chem. C, 2010, 114, 10088-10091.

- T. Xia, C. Zhang, N. A. Oyler and X. Chen, Adv. Mater., 2013, 25, 6905-6910.
- 65 16. Y.-F. Zhu, L. Zhang, T. Natsuki, Y.-Q. Fu and Q.-Q. Ni, ACS Appl Mater Interfaces, 2012, 4, 2101-2106.
- G. Sun, B. Dong, M. Cao, B. Wei and C. Hu, Chem. Mater., 2011, 23. 1587-1593
- 18. D. Zhang, F. Xu, J. Lin, Z. Yang and M. Zhang, Carbon, 2014, 80, 103-111.
- C. Wang, X. Han, P. Xu, J. Wang, Y. Du, X. Wang, W. Qin and T. Zhang, J. Phys. Chem. C, 2010, 114, 3196-3203.
- 20. J. Wei, T. Wang and F. Li, J. Magn. Magn. Mater., 2011, 323, 2608-
- 75 21. J. Liu, R. Che, H. Chen, F. Zhang, F. Xia, Q. Wu and M. Wang, Small, 2012, 8, 1214-1221.
 - C. Cui, Y. Du, T. Li, X. Zheng, X. Wang, X. Han and P. Xu, J. Phys. 22. Chem. B, 2012, 116, 9523-9531.
- 23. Y. Liu, Z. Zhang, S. Xiao, C. Qiang, L. Tian and J. Xu, Applied Surface Science, 2011, 257, 7678-7683.
- M. Zong, Y. Huang, Y. Zhao, X. Sun, C. Qu, D. Luo and J. Zheng, 24. RSC Adv., 2013, 3, 23638-23648
- 25. Y. Zhu, J. C. Zhang, J. Zhai, Y. M. Zheng, L. Feng and L. Jiang, ChemPhysChem, 2006, 7, 336-341.
- A. Das, H. T. Hayvaci, M. K. Tiwari, I. S. Bayer, D. Erricolo and C. 85 26. M. Megaridis, J. Colloid Interface Sci., 2010, 353, 311-315.
- 27. J. Xiao, G. Ouyang, P. Liu, C. X. Wang and G. W. Yang, Nano Lett, 2014, 14, 3645-3652.
- 28. M. H. Rümmeli, P. Ayala and T. Pichler, in Carbon Nanotubes and Related Structures, Wiley-VCH Verlag GmbH & Co. KGaA, 2010, ch1, pp. 1-21.
- 29. K. R. Paton and A. H. Windle, Carbon, 2008, 46, 1935-1941.
- R. C. Che, L. M. Peng, X. F. Duan, Q. Chen and X. L. Liang, Adv 30. Mate 2004, 16, 401-405.
- G. Wang, Z. Gao, S. Tang, C. Chen, F. Duan, S. Zhao, S. Lin, Y. 95 31. Feng, L. Zhou and Y. Qin, ACS Nano, 2012, 6, 11009-11017.
 - 32. Y. Naito and K. Suetake, IEEE Trans. Microw. Theory Tech., 1971, 19.65-72.